

Development of modularity in the neural activity of children's brains

Man Chen and Michael W. Deem
Department of Physics & Astronomy
Department of Bioengineering
Center for Theoretical Biological Physics
Rice University
Houston, TX 77005

Abstract. We study how modularity of the human brain changes as children develop into adults. Theory suggests that modularity can enhance the response function of a networked system subject to changing external stimuli. Thus, greater cognitive performance might be achieved for more modular neural activity, and modularity might likely increase as children develop. The value of modularity calculated from fMRI data is observed to increase during childhood development and peak in young adulthood. Head motion is deconvolved from the fMRI data, and it is shown that the dependence of modularity on age is independent of the magnitude of head motion. A model is presented to illustrate how modularity can provide greater cognitive performance at short times, i.e. task switching. A fitness function is extracted from the model. Quasispecies theory is used to predict how the average modularity evolves with age, illustrating the increase of modularity during development from children to adults that arises from selection for rapid cognitive function in young adults. Experiments exploring the effect of modularity on cognitive performance are suggested. Modularity may be a potential biomarker for injury, rehabilitation, or disease.

PACS numbers: 87.19.lw, 87.19.lv, 89.75.Fb, 89.75.-k

Keywords: fMRI, neural activity, modularity, development

Submitted to: *Phys. Biol.*

1. Introduction

A modular organization of neural activity can facilitate more rapid cognitive function, because much of the rewiring of connections required for adaptation is performed within the modules, which is easier and faster than within the entire network [1–7]. On the other hand, modularity may restrict possible cognitive function, because a modular neural architecture is a subset of all possible architectures [3–6]. Modularity in the neural activity of the human brain has been demonstrated [8, 9], with activation of neural activity in different parts of the brain observed by functional magnetic resonance imaging (fMRI) [10–16]. Remarkably, correlated neural activity can also be generated from free-streaming, subject-driven, cognitive states [10]. Models of developing neural activity have shown a self-organization of modular structure [17].

We here hypothesize that selection for neural responsiveness is strong during childhood and peaks during young adulthood. Since modularity increases responsiveness, we expect that modularity of neural activity in the brain might peak during adulthood as well. These modules are correlated with physical structure of the brain [18], but they are not completely hard coded at birth. Cognitive demands upon the brain promote development of modular neural activity, which empowers the brain with increased responsiveness and task switching ability.

A dynamic network of neural activity in the brain that can reconfigure its architecture will converge to a value of the modularity that depends on the pressure upon it [5, 6]. Here we show that modularity of neural activity in the human brain increases from age 4 and peaks in young adulthood. We use a model to interpret these results, showing that highly modular neural activity favors rapid, low-level tasks, whereas less modular neural activity promotes less rapid, effortful, high-level tasks. The model shows that increased connection between stored memories or faster required response times for adults versus children can explain the observed development of modularity in neural activity.

The structure of functional networks constructed from fMRI data is age dependent. For example, analysis of fMRI data from young adults and old adults shows the modularity of human brain functional networks decreases with age [6, 13, 19]. Additionally, the architecture of the default network of the brain extracted from fMRI

data changes as children develop into adults [20], and working memory performance has been shown to be related in an age-dependent way with functional networks [21]. That functional network constructed from fMRI data can be age dependent was emphasized in a study showing subject age can be estimated from 5 minutes of fMRI data from individual subjects [22]. These works suggest a clear developmental and age dependence of the networks constructed from fMRI data. In other work, connection matrices averaged over ages were constructed and the modularity of these average matrices was computed, observing no trend of modularity with age [23]. The lack of observed trend in that study may be due to the construction of averaged connection matrices, rather than consideration of the connection matrices constructed from each individual.

Measurements of task switching costs, both mixing and switching, show that young adults are more efficient than both children and old adults at task switching [24]. We suggest selection for neural task switching peaks during young adulthood, and that selection for task switching is one mechanism to explain the observed peak of modularity in neural activity in young adulthood. We demonstrate the cross-task utility of modularity in a model of memory recall. In other words, in this model, we show that modularity measured during the task of watching a movie has functional implications for a task such as memory recall. Previous results show that regions of interest observed during resting state activity strongly overlap with known functional regions [10, 18]. Thus, it is likely that the modularity observed during the task of movie watching has functional implications for other tasks, such as memory recall. Indeed, it has been demonstrated that modularity of resting-state neural activity is positively correlated with working memory capacity [25].

A number of studies have reported that children move their heads more than adults, and that this motion can affect properties computed from the observed fMRI data. Thus, it has been suggested that calculations should separately account for head motion and age when drawing conclusions about the effect of development on correlations of neural activity. In some subject populations, with particular alignment methods, spurious correlations between the computed network properties and extent of head motion have been observed [26]. Further work showed that the underlying age-dependent changes to the spatial dependence of correlations persist after head motion correction, although the magnitude of the age dependence decreases [27]. A study using the SPM2 software showed an apparent increase in local

connectivity and decrease in large-scale, distributed networks due to head motion [28]. A study using in-house software showed an effect of head motion on extracted time series data [29]. A study using FSL showed a negative correlation between modularity and head motion for motions above 0.07 mm [26]. Since head motion is negatively correlated with age, these studies caution that artifacts due to head motion might erroneously be interpreted to predict that modularity is positively correlated with age. We quantify head motion artifacts, showing that with the alignment procedure and strict censor cutoff used in our study, effects of head motion are negligible after alignment.

In this work, we analyzed patterns of neural activity measured by fMRI for children of different ages and for young adults watching a movie. We show that a mathematical definition of modularity, using several different basis sets, leads to the conclusion that modularity increases from childhood to young adulthood. These results are consistent with very recent results showing increased within-module connectivity during development [27]. Theory suggests that highly modular neural activity favors rapid, low-level tasks, whereas less modular neural activity promotes less rapid, effortful, high-level tasks [5, 6, 16]. We test the general predictions of this theory relating modularity to performance and we derive a fitness function for a quasispecies description of the modularity dynamics. We describe details of the data analysis in the Methods section. The Results section describes these results. In the Model section, we introduce a model to show that a more modular neural architecture leads to more accurate recognition of memory at short times. We also show that a more modular neural architecture leads to more accurate recognition of memories when stored memories are more overlapping. This model suggests that overlapping stored memories or faster required response times for adults versus children are mechanisms that could explain the observed development of near-resting state modularity in neural activity. We conclude with experimental and clinical implications in the Discussion section.

2. Methods

2.1. Subjects

We analyzed fMRI data from 21 adults age 18–26 and 24 children age 4–11 watching 20 minutes of Sesame Street [30]. Image acquisition details are provided in [30]. These data were taken from a set of 27 children (16 female) and 21 adults (13 female). Three children were excluded due to excessive head motion (> 5 mm), opting-out, or experimenter error. All children were typically developing. In addition, screening for neurological abnormalities was performed on all participants [30]. Raw, KBIT-2 overall IQ scores are known for 17 of the children and range from 18.5 to 66 [30].

2.2. Processing of fMRI Data

The two-dimensional fMRI data slices [30] were combined into a three-dimensional fMRI representation of the neural activity as a function of time, with 2 sec time resolution and 4 mm spatial resolution. The first six fMRI images of each subject were discarded to allow the blood oxygen level dependent (BOLD) signal to stabilize. The time series images for each subject were registered to 1 mm resolution, deskulled anatomical data, which created a normalized image in standard space. The time series images were then despiked, and the spike values were interpolated using a non-linear interpolation [31]. The images were then slice time corrected, registered, scaled into Talairach brain coordinates [32], motion corrected, bandpass filtered, and blurred (Cox, 1996). Frame-to-frame motion of a subjects' head was corrected by regressing out rigid translations and rotations of the fMRI data and derivatives of these parameters during the time course. Motion was censored with a threshold of 0.2, i.e. RMSD of 2 mm or 2 degrees based on the Euclidean Norm of the derivative of the translation and rotation parameters. Outliers were censored with a threshold of 10%. Due to excessive censoring, 2 of the child and 1 of the adult subject data were excluded. For the individuals remaining in the study, a small fraction of the time slices were removed by this censoring, also termed scrubbing, and the values replaced with values linearly interpolated from neighboring time points. All calculations were performed with AFNI [31]. The block of analysis code of example 9a in the `afni_proc.py` was applied.

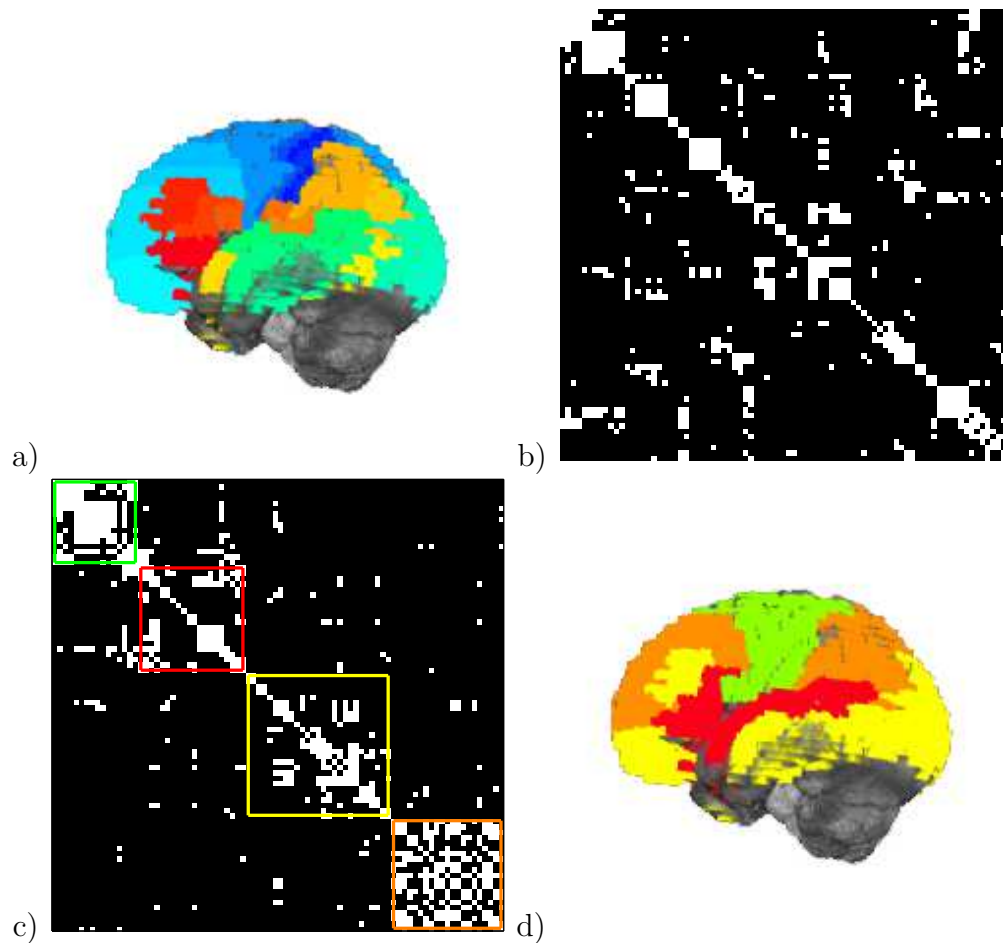


Figure 1. Brain neural activity is clustered into modules. a) fMRI neural activity data are projected onto Brodmann areas, shown as colored regions. b) Neural activity between different Brodmann areas is correlated for subjects watching 20 minutes of Sesame Street, shown here for one adult subject. Only the elements of the correlation matrix above a cutoff are retained (white). c) Modules are defined as the clusters that maximize Newman's modularity. The four modules identified from the 84 Brodmann areas for this subject are shown, of size 16 (green), 20 (red), 27 (yellow), and 21 (orange). The modularity is 0.6441, with contributions of 0.1585, 0.1310, 0.1592, and 0.1954 from each module respectively. d) The four modules of neural activity for this subject.

2.3. Calculation of Modularity

We computed modularity from correlations in neural activity of the brain extracted from fMRI data [11, 13, 33]. Fig. 1 illustrates the process. Correlations were computed for each subject between Brodmann areas, a standardized basis set describing regions of the human cerebral cortex [34]. Modularity was computed using the Newman algorithm [35]. We projected the N_{edge} largest values of the correlation matrix to unity, and set the remaining values to zero. We computed the modularity of this projected matrix. These values of modularity depend on the parameter N_{edge} , and it will be confirmed that adult modularity is greater than child modularity for all N_{edge} values. The value for the N_{edge} parameter must be large enough that the projected correlation matrix is fully connected, which implies $N_{\text{edge}} \geq 200$ for our data set. We considered $200 \leq N_{\text{edge}} \leq 500$ so that the non-linear effect of the projection were significant, i.e. the projected matrix was not simply all unity.

The numerical value of the modularity is the probability to have correlations within the modules, minus the probability expected for a randomized matrix with the same degree sequence [35]. In other words,

$$M = \frac{1}{2e} \sum_{\text{all modules}} \sum_{\text{areas } i,j \text{ within this module}} \left(A_{ij} - \frac{a_i a_j}{2e} \right) \quad (1)$$

where A_{ij} is one if there is an edge between Brodmann area i and Brodmann area j and zero otherwise, The value of $a_i = \sum_j A_{ij}$ is the degree of Brodmann area i , and $e = \frac{1}{2} \sum_i a_i$ is the total number of edges, as in Fig. 1. Edges are established if the correlation between Brodmann areas i and j is greater than the cutoff value, which is implicitly determined by the desired number of edges to keep in the matrix, see Fig. 1b. Modules are defined by the grouping that maximizes M [35]. The Newman algorithm [35] is used to calculate values of modularity and the identity of the modules. This algorithm gives a unique answer for the modularity and set of modules for a given connection matrix. The value of the modularity depends on how the Brodmann areas are grouped into modules, in Eq. 1, and the Brodmann areas are clustered into modules by choosing the grouping that maximizes the modularity, Eq. 1.

It is not necessary to use a cutoff in the calculation of the modularity. The Newman modularity calculation can be applied to a full matrix, with real number values,

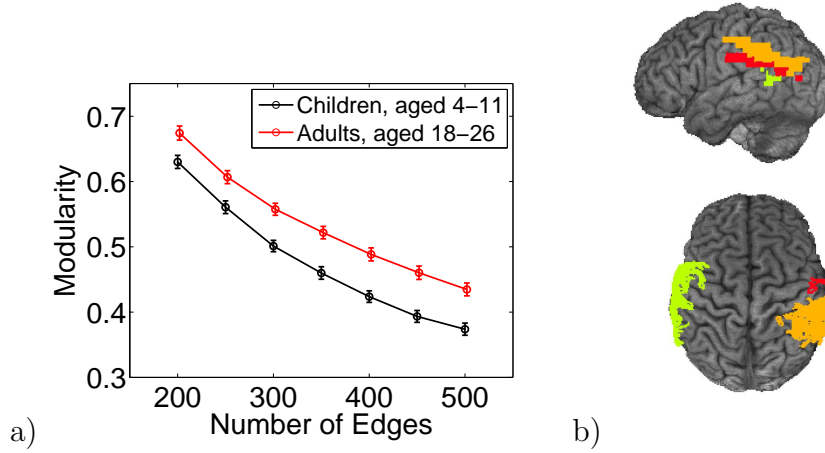


Figure 2. a) Average modularity of the neural activity in the brain for the child and adult cohorts. Modularity is greater for adults than for children. Modularity is computed from the correlation matrix of neural activity between Brodmann areas. The number of entries in the correlation matrix above the cutoff, denoted by edges, is chosen so that the matrix is fully connected yet still sparse. Modularity computed using different values of the cutoff persistently shows a higher value for adults than for children. The error bars are one standard error. b) top) The three Brodmann areas whose domains grow the most in size from children to adults, and bottom) the three Brodmann areas whose domains shrink the most, for 400 edges.

rather than the binary projection. That is, the matrix A in Eq. (1) can simply be the full correlation matrix, without projection. Modularity computations on the full, real-valued matrix will also be presented.

Finally, it is also not necessary to use the Brodmann areas as regions of interest. That is, the i and j in Eq. (1) can simply be voxels, rather than Brodmann areas. Results for $(8 \text{ mm})^3$ and $(12 \text{ mm})^3$ voxels will be presented. Thus, modularity values for three different basis sets were computed.

3. Results

Figure 2a shows modularity of neural activity for children and adults. The modularity of neural activity of adults is greater than that of children (p -value

Table 1. Quantification of the persistence of modularity and module identity with optimization of modularity.

| Dependent variable and independent variable(s) | R^2 | p -value | $\partial M / \partial \text{age}$ |
|---|--------|------------|------------------------------------|
| M with age | 0.1904 | 0.0211 | 0.0102 |
| M with EN | 0.0158 | 0.2897 | |
| EN with age | 0.0071 | 0.3545 | |
| M with age and EN | 0.2170 | 0.0490 | 0.0106 |

< 0.001 for 400 edges). This result persists when different cutoff values are used to calculate modularity from the correlation matrix. The results for 400 edges are representative, and unless otherwise noted, we used this criterion to construct the projected correlation matrix. Modularity of neural activity increases with age during childhood development. The average Pearson correlation between modularity and age, corresponding to the data in Fig. 2a, is 0.44 (p -value 0.02, sample size 22). Similarly, the average Pearson correlation between modularity and raw, not-age-normalized KBIT-2 overall IQ score is 0.234 (p -value 0.16, sample size 16, as some children did not have reported IQ scores). The positive correlation of modularity with both age and raw IQ shows the development of modularity in neural activity in the brain during childhood.

3.1. Modularity of a Full Matrix with Real-Numbered Connection Weights

Figure 3 shows the results when the full matrix is computed, the ‘‘Brodmann area’’ values. The modularity of adults and children are significantly different, p -value 7×10^{-5} .

3.2. Effect of Head Motion on Calculation of Modularity.

The extent of head motion was measured by the Euclidean norm of the derivatives of the motion parameters, termed EN. To illustrate this point, a number of correlations were carried out to illustrate the effect of head motion. The correlations for children are shown in Table 1 and Fig. 4. Modularity is significantly correlated with age.

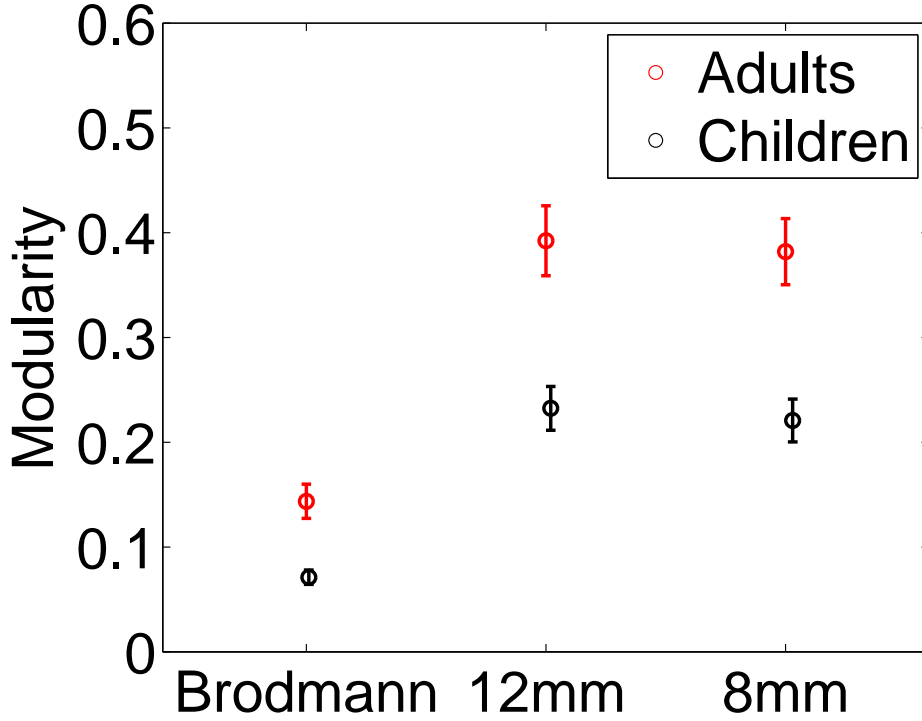


Figure 3. Calculation of modularity when the full matrix of correlations is used. Calculations were performed using Brodmann areas as nodes and a 84×84 matrix of correlations. Calculations were also performed without masking the data to Brodmann areas, and using the original data at a resolution of 12 mm and a 2160×2160 correlation matrix or a resolution of 8 mm and a 6426×6426 correlation matrix. The p -values for the significance of the difference between the modularity of adults and children are 7×10^{-5} , 9×10^{-5} , and 4×10^{-5} , respectively. These results confirm the generality of the results in Fig. 2. Modularity develops during childhood.

Furthermore, inclusion of EN to the correlation of modularity with age only very slightly increases the goodness of fit (R^2), and does not change the positive slope of the correlation of M with age. The coefficient relating modularity to age, $\partial M / \partial \text{age}$, is the same whether head motion is included as an independent variable or not. Thus, the head motion is not biasing the estimated relationship between modularity and age. The correlations of modularity or age with EN are small and not significant. The correlation of modularity with EN for adults is also small and not significant,

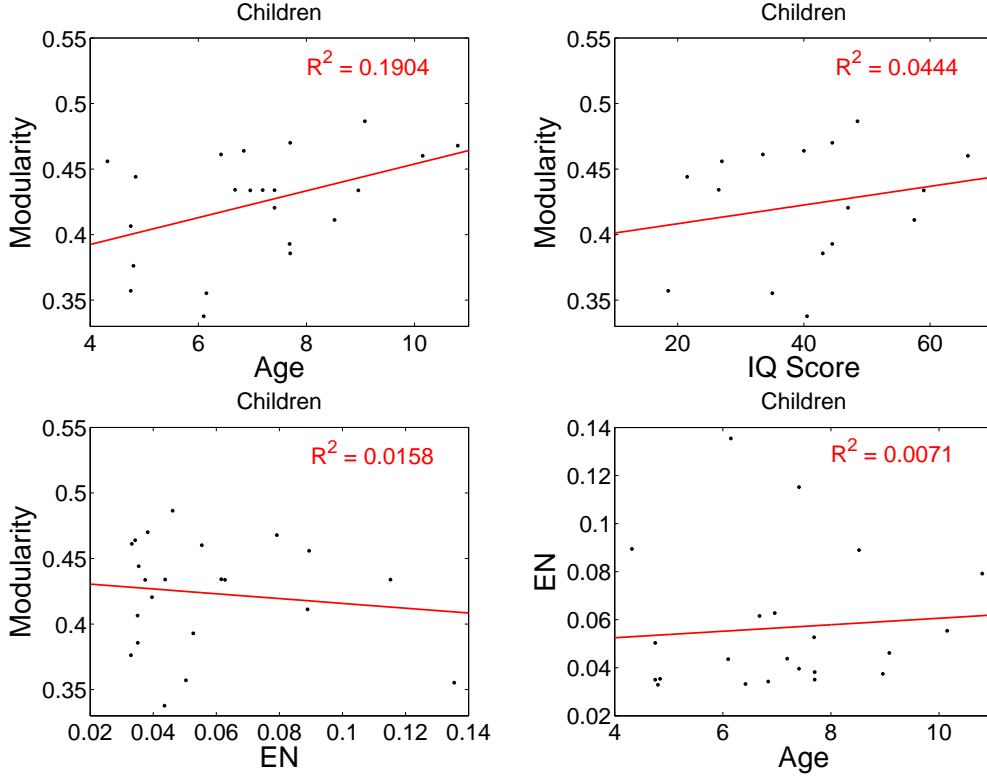


Figure 4. The correlation of modularity with age, IQ score, and Euclidean norm (EN) from AFNI for children. Also shown is the correlation of EN with age.

p -value = 0.32.

3.3. Development of Modules

Not only is the modularity of neural activity in the children and adults different, but also the identity of the modules changes with development. We computed the probability that Brodmann areas i and j were in the same module, as estimated from the data by the observed fraction. Consider a single person. The probability that area i and j are in the same module, p_{ij} , is either 0 or 1 (they either are, or are not, in the same module in one given subject sample). The sum of this quantity over j is the size of the module in which i is a member, S_i . Averaging S_i over all children or all adults gives the average size of the module in which i participates, $\langle S_i \rangle_{\text{child}}$ or

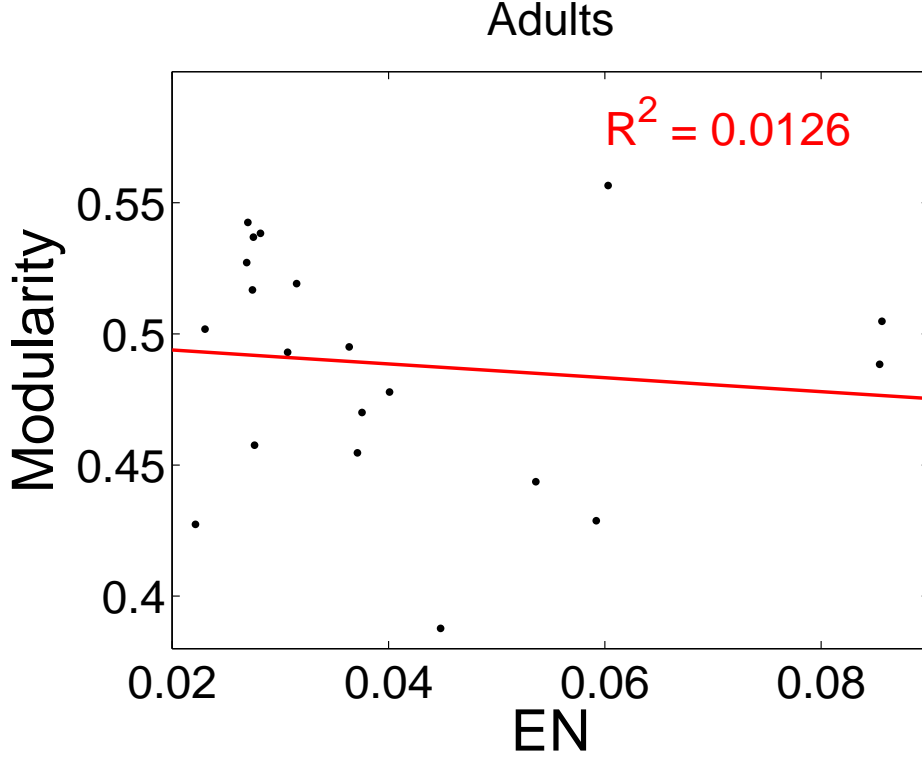


Figure 5. The correlation of modularity with Euclidean norm from AFNI (EN) for adults. The correlation is small and not significant, p -value = 0.32.

$\langle S_i \rangle_{\text{adult}}$, respectively. These two quantities were calculated for each Brodmann area. Also reported are the three i for which $\langle S_i \rangle_{\text{adult}} - \langle S_i \rangle_{\text{child}}$ is largest and the three i for which $\langle S_i \rangle_{\text{adult}} - \langle S_i \rangle_{\text{child}}$ is smallest.

We found the three Brodmann areas that had the largest positive difference between the average module size in adults and children, shown in Fig. 2b. These are the areas whose modules grew most in size with development. They are left Brodmann area 23, 29, and 31. We also found the three Brodmann areas that had the largest negative difference in average module size between adults and children, i.e. the areas whose modules shrink most with development, shown in Fig. 2b. They are left Brodmann area 21, right 40, and right 43.

Table 2. Quantification of modularity and module identity persistence with optimization of modularity.

| T | $\langle Q \rangle$ (adults) | $\langle Q \rangle$ (children) | (Number top areas in common with $T = 0$ case)/3 | (Number of bottom areas in common with $T = 0$ case)/3 |
|------|---------------------------------|-----------------------------------|--|--|
| 0 | 0.4885 | 0.4237 | 1.00 | 1.00 |
| 0.01 | 0.4885 | 0.4237 | 1.00 | 0.65 |
| 0.05 | 0.4883 | 0.4233 | 0.97 | 0.62 |
| 0.10 | 0.4871 | 0.4220 | 0.86 | 0.60 |

3.4. Near Degeneracy of Modularity Values

In the definition of modularity, Eq. (1), there can be partitions that give values of modularity near but slightly below the optimal value. The optimal value is denoted by M , and the nearby values are denoted by Q . To address the near degeneracy of modularity values, that is values of Q that are near the optimal value of modularity M , the Newman algorithm was generalized to include the possibility of accepting a move that decreases Q , with probability $\min[1, \exp(\Delta Q/T)]$. This generalization leads to sampling the near-optimal values of Q , roughly in the range $M - T$ to M . How the average Q varies with T was calculated. Also calculated was how often the set of the 3 Brodmann areas for $\langle S_i \rangle_{\text{adult}} - \langle S_i \rangle_{\text{child}}$ is largest changes identity in 100 runs, and similarly for the set of the 3 for which it is smallest. From these results, one sees that M values reported are representative, i.e. the nearly degenerate $\langle Q \rangle$ values are close to the optimal value, M . The identification of 3 Brodmann areas for which $\langle S_i \rangle_{\text{adult}} - \langle S_i \rangle_{\text{child}}$ is largest and the 3 for which it is smallest is relatively stable among these nearly degenerate states. Essentially only the least stable member of the latter is lost at finite T (3/3 and 2/3 of the members are stable, respectively). The top areas are more stable than the bottom areas, because there is a gap in the distribution of $\langle S_i \rangle_{\text{adult}} - \langle S_i \rangle_{\text{child}}$ after the 3rd highest value, see Fig. 6. This distribution shows there is a natural set of highest and lowest outliers.

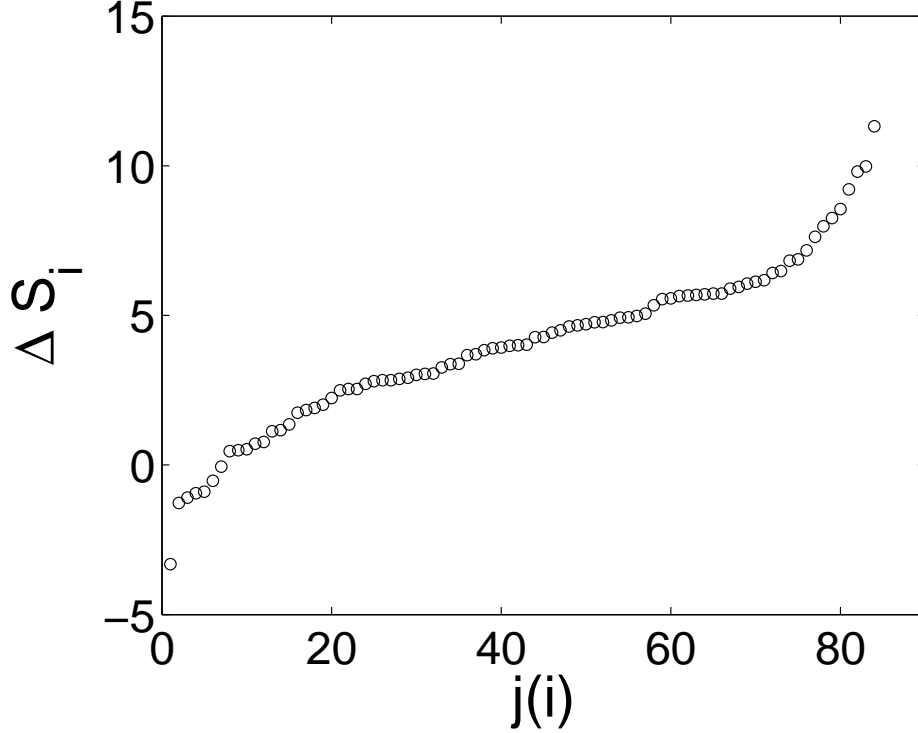


Figure 6. The distribution of the values of $\langle S_i \rangle_{\text{adult}} - \langle S_i \rangle_{\text{child}}$. They are ordered from smallest to largest; $j(i)$ denotes this ordering.

4. Model

4.1. Model of the Response Function for Memory Recall

We will explore a mechanism to understand the results with a model of neural activity and cognitive function. We build upon the Hopfield neural network model [36]. Models of brain activity with different levels of detail and complexity have been developed. At the detailed level, there are models of individual neuron activation and spiking [37–39]. These models have been generalized to a population of neurons, in which synchronization of the spike trains has been calculated [40, 41]. The data analyzed are at the resolution of 4 mm, and a voxel of $(4 \text{ mm})^3$ contains roughly a million neurons. The modeling is, therefore, of interactions between groups of

neurons, with each group containing a million neurons. In addition, the time resolution of the fMRI BOLD signal data is 2 s. The fMRI BOLD signal results from the difference in magnetic spin properties of oxygenated and deoxygenated hemoglobin. This signal is, therefore, a representation of blood flow to each region of the brain. The regional blood flow is an indication of local neural activity [42]. At this time and length scale, a model such as the Hopfield neural network is appropriate. As with the data, neural activity is the only observable in this model.

We used a neural network model to describe the dynamics of neural activation that was measured by the fMRI experiments. The voxels of neural activation measured in the fMRI are subgroups of neurons in the brain. In the model, the activation state of subgroup i is given by $\sigma_i(t)$, which takes on values 1 or -1 to indicate that the subgroup of neurons is active or inactive on average at time t , respectively. Thus, for each physical region of the brain in Fig. 1a, there is a $\sigma_i(t)$. The neural state at time $t + 1$ was created from the neural state at time t , based upon connections between neurons and stored memories. We here took the connections between the neurons to be modular, with modularity M . These functional connections, denoted by the matrix A_{ij} below, correspond roughly to the modules identified in Fig. 1d. The model describes how neural states in the brain are driven to match stored patterns, with the μ th pattern denoted by ξ_i^μ . We also took the stored memories to be clustered. The correlation between these stored patterns is denoted by the weight matrix W_{ij} . The clustering of the stored memories is quantified a parameter p , described below. The modules identified in the fMRI experiments, Fig. 1d, are described in detail in the model through the combined influence of the connection matrix and the memory correlation matrix, $A_{ij}W_{ij}$.

We related the modularity of the neural activation in the model to the modularity of the neural activity as measured by fMRI. The connection matrix denotes whether neural region i is connected to region j . Due to physiological changes that occur during development, these connections change, as shown in Figs. 2 and 3. In particular, we set the connection matrix of the neural network to be modular [43], with modularity M . Crucially, we also set the stored memory patterns to be clustered as well, with modularity p . The neural state is propagated from a random initial state to recall a stored memory according to the Hebbian learning rule [44]. We computed the average overlap between the final neural state and the stored memory. In terms of an experiment, overlap at time t can be interpreted as quantifying how

well a subject correctly identifies an image that is visible for a time, t .

In the neural network model, memory μ is defined by the pattern $\xi_i^\mu = \pm 1$ of length $N = 256$ bits [36]. The weight matrix is defined by $W_{ij} = \sum_\mu \xi_i^\mu \xi_j^\mu$. The $N/4 \times N/4$ block diagonals define the four modules. Four distinct patterns are stored, one per module. Each pattern μ has $N/4$ values with $\xi_i^\mu = +1$, each of which has probability $(1 + 3p)/4$ of being within the μ^{th} block diagonal. The neural state is defined by $\sigma_i(t)$ and updated by the Hebbian learning rule [44] $\sigma_i(t+1) = \text{sign}[\sum_j A_{ij} W_{ij} \sigma_j(t)]$. The connection matrix A is binary and sparse, with average degree $\langle k \rangle = 30$. The probability for a connection to be at a given site within the block diagonal is given by $(1 + 3M)\langle k \rangle/N$. The overlap of the neural state with the target memory is given by $\max_\mu \sum_i \xi_i^\mu \sigma_i(t)/N$.

4.2. A Hierarchical Generalization

It has been argued that at the largest scales, the brain structure is hierarchical, not simply modular. Thus, the modular Hopfield neural network described above was also generalized to an hierarchical model. A similar hierarchical model was studied by Rubinov *et al.* in a computational analysis to show the effect of self-organized criticality and neuronal information processing [41]. In the modular model, the connection matrix A is made modular. In the hierarchical model discussed here, 5 levels, γ , are defined. The level for matrix position ij is defined as the smallest γ for which $\lfloor i/4^\gamma \rfloor = \lfloor j/4^\gamma \rfloor$. For example, $\gamma = 0$ is the diagonal, and $\gamma = 4$ is the entire matrix, excluding the all the 4×4 block diagonals. See Fig. 7. The probability to be within region γ is assigned to be proportional to $1 - \gamma\epsilon$, with the proportionality determined so that the average number of connections per node remains at 30. Here $\epsilon = 1/4$ is a measure of the asymmetry introduced by the hierarchy.

4.3. Model Results

The cognitive ability of the brain, i.e. its ability to solve a challenge, depends on modularity of the neural activity. The responses of the model neural system with high modularity and lower modularity are shown in Fig. 8. In this figure, cognitive performance is quantified by overlap between evolved neural state and target memory

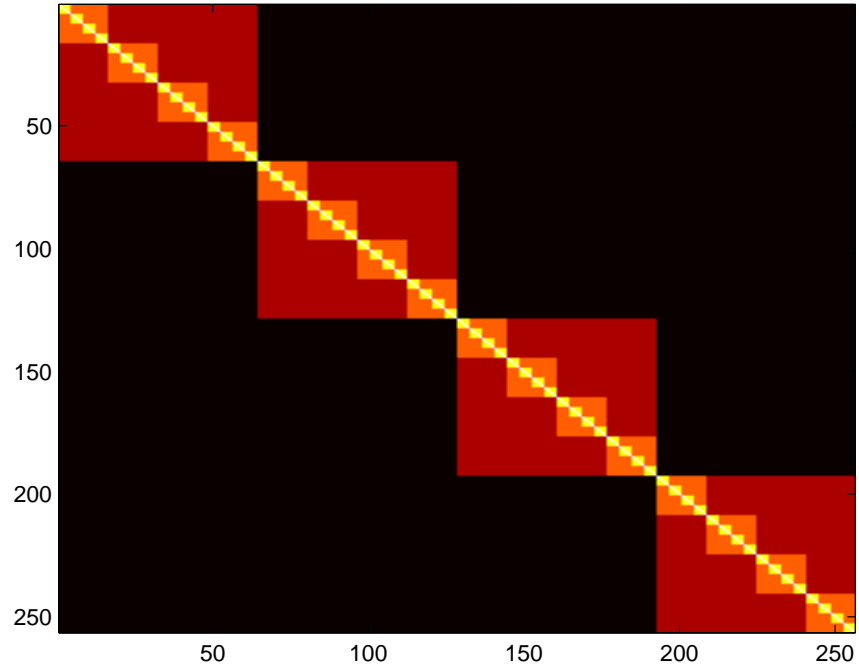


Figure 7. Pictorial representation of the hierarchical matrix. The levels are 4 (black), 3 (red), 2 (orange), 1 (yellow), and 0 (white). matrix.

state. These performance curves as a function of time and neural architecture depend on the clustering of the stored memories, p . The overlap typically increases with time, as the target memory is dynamically recalled. At short times, a more modular memory architecture can lead to a better recall, i.e. greater overlap with the stored memory. At longer times, a less modular memory architecture can give better performance. We view this crossing of the performance as a function of time to be a generic result of an evolving dynamical system with a rugged fitness landscape [45] and not unique to the particular model used here.

The variation in performance, shown in Fig. 8, helps to explain the change of modularity during development. We use quasispecies theory to quantify the relationship between performance and change of modularity. In this theory, systems with different modularity, m , are assigned a fitness, $f(m)$, that quantifies the benefit

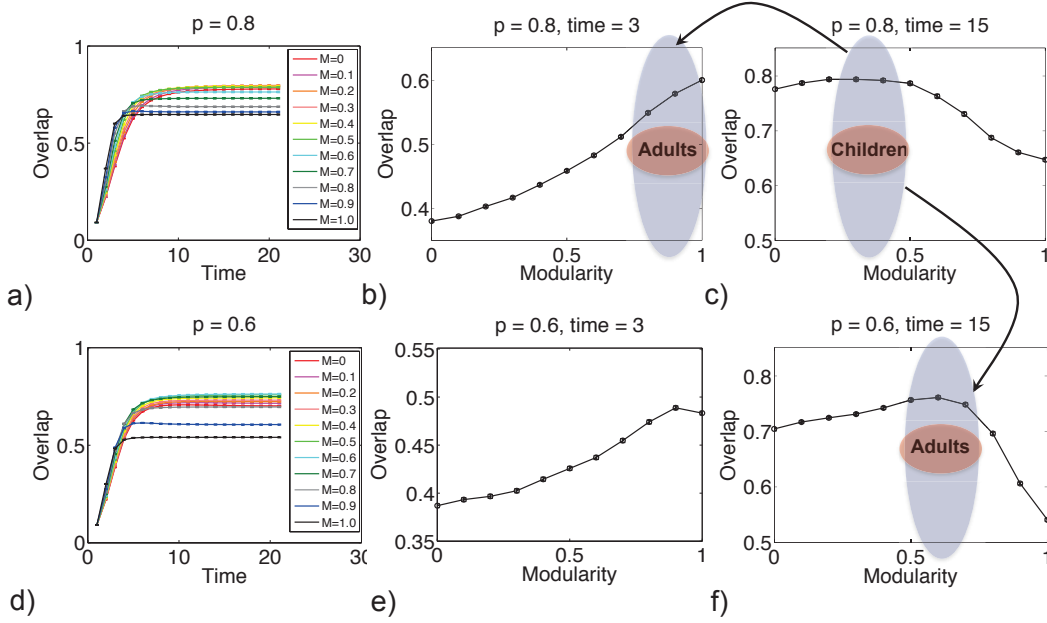


Figure 8. More modular neural architectures give better performance at short times (a or d, short time) and less modular memory architectures can give better performance at long times (a or d, long time). The greater modularity in adults than children, Fig. 2, is consistent with either cognitive performance at short times is more important in adults than children (top arrow) or that memories are less clustered in adults than children (bottom arrow). Overlap is a measure of the probability that the neural state correctly recalls a memory. The modularity of the connection matrix is M . The timescale is of order seconds. The clustering of the stored patterns is denoted by p .

of performance. This theory predicts how modularity changes with time, given the fitness function, and the rate at which entries in the connection matrix change, μ .

We take the overlap in Fig. 8 as the fitness for modularity, $f(m)$, in the brain and use quasispecies theory [46] to predict how modularity develops with age. The average modularity, $M(t) = \langle m(t) \rangle$, changes with age according to

$$\frac{dM}{dt} = N \langle m f[p(t), m] \rangle - NM \langle f \rangle - \mu M \quad (2)$$

where μ is the rate of mutations in the connection matrix [46]. Following the bottom

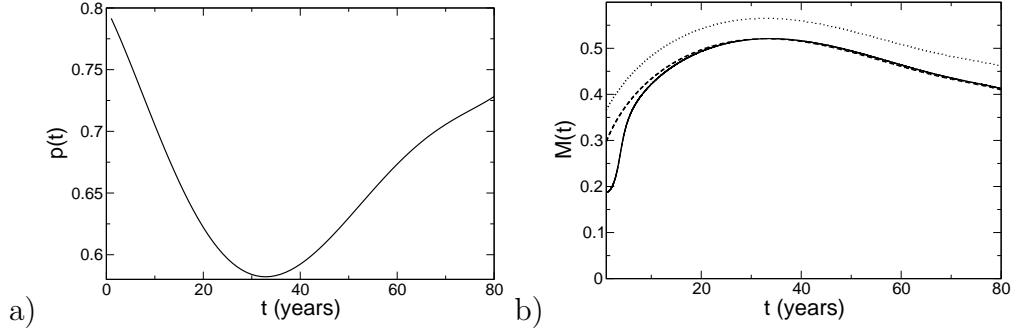


Figure 9. a) The clustering of memories versus age, after the bottom arrow in Fig. 8. b) The average modularity versus age predicted by quasispecies theory (solid). Here, the fitness is $10\times$ the overlap in Fig. 8, and the rate of mutation is $\mu = 0.1$ [46]. Also shown is the adiabatic approximation to the modularity, M^∞ (dashed) as well as the modularity that maximizes the fitness, M^* (dotted).

arrow of Fig. 8, the response time is taken to be 15, and it is assumed that $p(t)$ changes from 0.8 at birth to 0.6 in middle age and 0.7 in old age, This $p(t)$ is shown in Fig. 9a. Previous studies have shown that the modularity, measured with an automated anatomical labeling (AAL) basis set for resting state activity, of neural activity in adults with average age of 70 is roughly 7% below that of adults with average age of 22 [6, 13]. Another study of 193 adults aged 34–87, also using the AAL basis set, found that on average, modularity decreased 8% over 50 years [19]. These results imply p should be lower in old age than in young adulthood. The prediction from Eq. (2), shown in Fig. 9b, is a qualitative prediction for the developing human brain. Due to mutation [46], the observed modularity in Fig. 9b is below the value that maximizes the fitness, $M^*(t)$, defined by $f[p(t), M^*(t)] \geq f[p(t), M] \forall M$. We calculate the modularity in the adiabatic limit, $M^\infty(t)$, from the steady-state average fitness derived from a solution of the quasispecies theory [46]:

$$\begin{aligned}
 f_{\text{pop}} &= \max_{\xi} \{ f[p(t), \xi] - \mu C [(N - L)L/N^2][2 + (N/L - 2)\xi] \\
 &\quad - 2\sqrt{(1 - \xi)(1 + (N/L - 1)\xi)} \} \\
 &= f[p(t), M^\infty(t)]
 \end{aligned} \tag{3}$$

where C is the average number of connections in the connection matrix, per row.

Results for the hierarchical model, analogous to those in Fig. 2, are shown in Figs.

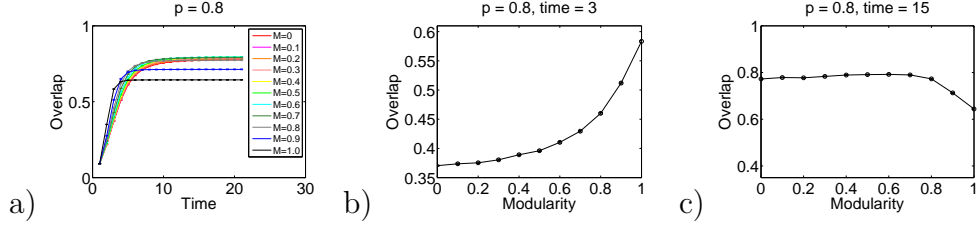


Figure 10. Hierarchical Hopfield model results. Here $p = 0.8$.

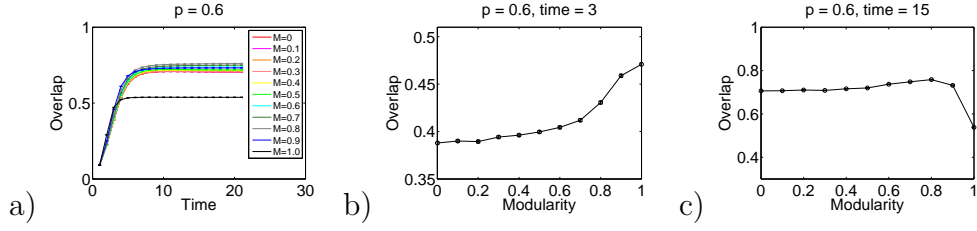


Figure 11. Hierarchical Hopfield model results. Here $p = 0.6$.

10 and 11. These results show that this hierarchical generalization of the Hopfield model also shows a crossing of the response function at intermediate times. That is, low levels of hierarchy lead to better responses at long times. And high levels of hierarchy can lead to better responses at short times.

5. Discussion

We have observed that modularity of neural activity in the brain increases with age from children to young adults, as measured by fMRI experiments. These data are summarized in Fig. 2. The analysis separately takes into account head motion, and the present study finds that after censoring and alignment, the effects of head motion are negligible.

The N_{edge} cutoff parameter from Fig. 2 can be viewed as a clustering parameter. What Fig. 2 shows is that the modularity of adults is greater than that of children, persistently with the value of the N_{edge} cutoff parameter. In other words, the conclusion that modularity develops from children to adults is robust with respect to the particular value of the cutoff parameter.

Previous analysis of fMRI data from young adults and old adults has shown that modularity of neural activity in the brain decreases with age [6, 13, 19]. Taken together with the present results, it appears that modularity of neural activity peaks in young adulthood.

The calculation of modularity was done using both the Brodmann areas as a basis and using raw voxel data. Both calculations show the modularity of children is greater than that of young adults. Additionally, the calculated values of modularity were shown to be representative of the full distribution of near-optimal values.

The Brodmann areas that grew most during development, left Brodmann area 23, 29, and 31, are in the posteromedial cortex. They play a central role in the brain neural network and in communication with the rest of the brain [47–49]. These areas also play important roles in memory retrieval [50, 51]. It is interesting that all three areas in the left brain, generally associated with logic, language and analytical thinking. The Brodmann areas identified to be in the modules that grow the most with development are somewhat sensitive to the number of edges used in the projection of the correlation matrix. For the range of edges show in Fig. 2a, 80% of the identified Brodmann areas are in the left hemisphere. Additionally, the area with the most dominantly growing module, left Brodmann 29, is identified 80% of the time. Our results are consistent with the observation that the right brain is dominant in infants, and that left brain develops later into adulthood [52]. The Brodmann areas that shank most during development, They are left Brodmann area 21, right 40, and right 43, are related to language perception and processing, accessing word meaning, and face recognition [53, 54]. The area with the most dominantly shrinking module, left Brodmann 21, is identified 80% of the time.

Prior results show that young adults are able to more quickly solve task-switching challenges than are children or old adults [24]. The present model shows that modularity allows for rapid responses. That is, a more modular neural activity can allow the brain to switch more quickly from one type of neural activation to another. This conclusion is robust to refinements in the hierarchical structure of the model. Therefore, selective pressure for rapid cognition should lead to the emergence of modularity in neural activity of the brain during childhood development.

The present model suggests that modularity of neural activity may develop to facilitate rapid cognitive function. Modularity may be larger in young adults than

in children because the typical required response time is shorter (upper arrow of Fig. 8). Modularity may also be larger because there are more connections between memories in adults than children, i.e. memories are less clustered, quantified by a smaller p (lower arrow Fig. 8). A module offers a pre-computed solution to a problem that has been previously encountered. Development of modularity from children to adults, thus, can improve task-switching performance.

5.1. Experimental Implications

Experiments to determine cognitive performance, as it depends on modularity, would be interesting to carry out. Predictions from quasispecies theory using this fitness function could test the significance of the measured task for developmental selection. Cognitive performance of subjects could be challenged while fMRI data are collected. For example, as suggested by the model, the probability of a subject to correctly identify an image visible for a time t may be measured. The cognitive performance should depend, among other parameters, on the modularity of the correlations in the subject's neural activity in the brain. Measuring performance as a function of modularity would provide the cognitive performance function, e.g. Fig. 8a or d, for this particular task. Perhaps the cognitive performance function will peak at different values of modularity for different tasks. It has been suggested that cognitive processes which are fast are more modular than those which are slow [16]. The results in Fig. 8 show why this is the case: modular networks provide better performance at short times (Fig. 8b or e), but less modular networks can provide better performance at long times (Fig. 8c or f). Measurements of cognitive performance for high-level and low-level tasks would complement these results. We predict that performance curves as a function of time will cross for subject samples with different values of modularity, as in Fig. 8a.

5.2. Modularity as a Biomarker

A biomarker for brain function may be developed from modularity. For example, modularity of neural activity in epileptic patients is less than that in normal subjects [15]. Anecdotal evidence [55] suggests that neural activity in patients with traumatic brain injury (TBI) is less modular than that in healthy subjects. Thus, we predict

that background neural activity in the brains of TBI patients will be less modular than that of healthy subjects. If so, modularity may be useful to quantify the extent of TBI, which is currently difficult to determine. Effectiveness of treatment is also difficult to quantify, and measurements of modularity may be helpful to track progress of TBI rehabilitation treatments. Measurements of modularity may even be useful as feedback during treatment. Interestingly, modularity seems to increase in response to disease progression and reduced cognitive function in multiple sclerosis patients [56], perhaps because the system is compensating for increased stress due to reduced function with increased modularity [6].

Acknowledgments

We thank Jessica Cantlon for providing the fMRI, age, and IQ data [30]. This research was supported by the US National Institutes of Health under grant 1 R01 GM 100468–01.

References

- [1] Wagner G P and Altenberg L 1996 Complex adaptations and the evolution of evolvability *Evolution* **50** 967–976
- [2] Lipson H, Pollack J B and Suh N P 2002 On the origin of modular variation *Evolution* **56** 1549–1556
- [3] Kashtan N and Alon U 2005 Spontaneous evolution of modularity and network motifs *Proc. Natl. Acad. Sci. USA* **102** 13773–13778
- [4] Kashtan N, Noor E and Alon U 2007 Varying environments can speed up evolution *Proc. Natl. Acad. Sci. USA* **104** 13711–13716
- [5] Sun J and Deem M W 2007 Spontaneous emergence of modularity in a model of evolving individuals *Phys. Rev. Lett.* **99** 228107
- [6] Lorenz D M, Jeng A and Deem M W 2011 The emergence of modularity in biological systems *Phys. Life Rev.* **8** 129–160

- [7] Callahan B, Thattai M and Shraiman B I 2009 Emergent gene order in a model of modular polyketide synthases *Proc. Natl. Acad. Sci. USA* **106** 19410–19415
- [8] Mountcastle V B 1979 An organizing principle for cerebral function: The unit module and the distributed system *The Neurosciences Fourth Study Program* (MIT Press) pp 21–42
- [9] Fodor J 1983 *The Modularity of Mind* (MIT Press)
- [10] Shirer W R, Ryali S, Rykhlevskaia E, Menon V and Greicius M D 2012 Decoding subject-driven cognitive states with whole-brain connectivity patterns *Cerebral Cortex* **22** 158–165
- [11] Schwarz A J, Gozzi A and Bifone A 2008 Community structure and modularity in networks of correlated brain activity *Magnetic Resonance Imaging* **26** 914–920
- [12] Ferrarini L *et al.* 2009 Hierarchical functional modularity in the resting-state human brain *Human Brain Mapping* **30** 2220–2231
- [13] Meunier D, Achard S, Morcom A and Bullmore E 2009 Age-related changes in modular organization of human brain functional networks *NeuroImage* **44** 715–723
- [14] He Y *et al.* 2009 Uncovering intrinsic modular organization of spontaneous brain activity in humans *PLoS ONE* **4** e5226
- [15] Chavez M, Valencia M, Navarro V, Latora V and Martinerie J 2010 Functional modularity of background activities in normal and epileptic brain networks *Phys. Rev. Lett.* **104** 118701
- [16] Meunier D, Lambiotte R and Bullmore E T 2010 Modular and hierarchically modular organization of brain networks *Front. Neurosci.* **4** 200 doi: 10.3389/fnins.2010.00200
- [17] Rubinov M *et al.* 2009 Symbiotic relationship between brain structure and dynamics *BMC Neurosci.* **10** 55
- [18] Hermundstad A H *et al.* 2013 Structural foundations of resting-state and task-

- based functional connectivity in the human brain *Proc. Natl. Acad. Sci. USA* **110** 6169–6174
- [19] Onoda K and Yamaguchi S 2013 Small-worldness and modularity of the resting-state functional brain network decrease with aging *Neurosci. Lett.* **556** 104–108
- [20] Fair D A *et al.* 2008 The maturing architecture of the brain’s default network *Proc. Natl. Acad. Sci. USA* **105** 4028–4032
- [21] Satterthwaite T D *et al.* 2013 Functional maturation of the executive system during adolescence *J. Neurosci.* **33** 16249–1626
- [22] Dosenbach N U F *et al.* 2010 Prediction of individual brain maturity using fMRI *Science* **329** 1358–1361
- [23] Fair D A *et al.* 2009 Functional brain networks develop from a ‘local to distributed’ organization *PLoS Comput. Biol.* **5** e1000381
- [24] Karbach J and Kray J 2009 How useful is executive control training? age differences in near and far transfer of task-switching training *Develop. Sci.* **12** 978–990
- [25] Stevens A A, Tappin S C, Garg A and Fair D A 2012 Functional brain network modularity captures inter- and intra-individual variation in working memory capacity *PLoS ONE* **7** e30468
- [26] Satterthwaite T D *et al.* 2012 Impact of in-scanner head motion on multiple measures of functional connectivity: Relevance for studies of neurodevelopment in youth *NeuroImage* **60** 623–632
- [27] Satterthwaite T D *et al.* 2013 Heterogeneous impact of motion on fundamental patterns of developmental changes in functional connectivity during youth *NeuroImage* **83** 45–57
- [28] Van Dijk K R A, Sabuncu M R and Buckner R L 2012 The influence of head motion on intrinsic functional connectivity MFI *NeuroImage* **59** 431–438
- [29] Power J D *et al.* 2012 Spurious but systematic correlations in functional connectivity MFI networks arise from subject motion *NeuroImage* **59** 2142–2154

- [30] Cantlon J F and Li R 2013 Neural activity during natural viewing of sesame street statistically predicts test scores in early childhood *PLoS Biology* **11** e1001462
- [31] Cox R W 1996 AFNI: Software for analysis and visualization of functional magnetic resonance neuroimages *Comput. Biomed. Res.* **29** 162–173
- [32] Talairach J and Tournoux P 1988 *Co-planar stereotaxic atlas of the human brain* (Thieme)
- [33] Fortunato S 2010 Community detection in graphs *Phys. Rep.* **486** 75–174
- [34] Nolte J 2008 *Nolte's The Human Brain: An Introduction to its Functional Anatomy* 6th ed (New York: Mosby)
- [35] Newman M E J 2006 Modularity and community structure in networks *Proc. Natl. Acad. Sci. USA* **103** 8577–8582
- [36] Hopfield J J 1982 Neural networks and physical systems with emergent collective computational abilities *Proc. Natl. Acad. Sci. USA* **79** 2554–2558
- [37] FitzHugh R 1961 Impulses and physiological states in theoretical models of nerve membrane. *Biophysical J.* **1** 445–466
- [38] Nagumo J, Arimoto S and Yoshizawa S 1962 An active pulse transmission line simulating nerve axon *Proc. IRE* **50** 2061–2070
- [39] Wang X J and Buzsáki G 1996 Gamma oscillation by synaptic inhibition in a hippocampal interneuronal network model *J. Neurosci.* **16** 6402–6413
- [40] Buzsáki G and Wang X J 2012 Mechanisms of gamma oscillations *Ann. Rev. Neurosci.* **35** 203–225
- [41] Rubinov M *et al.* 2011 Neurobiologically realistic determinants of self-organized criticality in networks of spiking neurons *PLoS Comput. Biol.* **7** e1002038
- [42] Ogawa S, Lee T M, Nayak A S and Glynn P 1990 Oxygenation-sensitive contrast in magnetic resonance image of rodent brain at high magnetic fields *Magnetic Resonance in Medicine* **14** 68–78

- [43] Pradhan N, Dasgupta S and Sinha S 2011 Modular organization enhances the robustness of attractor network dynamics *Euro. Phys. Lett.* **94** 38004
- [44] Amit D J 1989 *Modeling Brain Function* (Cambridge: Cambridge University Press)
- [45] Deem M W 2013 Statistical mechanics of modularity and horizontal gene transfer *Ann. Rev. Cond. Matt. Phys.* **4** 287–311
- [46] Park J M, Niestemski L R and Deem M W 2014 Quasispecies theory for evolution of modularity ArXiv:1211.5646
- [47] Leech R, Braga R and Sharp D J 2013 Echoes of the brain within the posterior cingulate cortex *J. Neurosci.* **32** 215–222
- [48] Nielsen F A, Balslev D and Hansen L K 2005 Mining the posterior cingulate: segregation between memory and pain components *Neuroimage* **27** 520–532
- [49] Kozlovskiy S A, Vartanov A V, Nikonova E Y, Pyasik M M and Velichkovsky B M 2012 The cingulate cortex and human memory processes *Psychology in Russia: State of the Art* **5** 231–243
- [50] Cavanna E A and Trimble M R 2006 The precuneus: A review of its functional anatomy and behavioral correlates *Brain* **129** 564–583
- [51] Parvizi J, Hoesen G W V, Buckwalter J and Damasio A 2006 Neural connections of the posteromedial cortex in the macaque *Proc. Natl. Acad. Sci. USA* **103** 1563–1568
- [52] Chiron C, Jambaque I, Nabbout R, Lounes R, Syrotal A and Dulac O 1997 The right brain hemisphere is dominant in human infants *Brain* **120** 1057–1065
- [53] Stoeckel C, Cougn P M, Watkins K E and Devlin J T 2009 Supramarginal gyrus involvement in visual word recognition *Cortex* **45** 1091–1095
- [54] Technologies T C 2012 *Cortical Function Reference*
- [55] Leclercq M *et al.* 2000 Dual task performance after severe diffuse traumatic brain injury or vascular prefrontal damage *J. Clin. Exper. Neuropsychol.* **22** 339–350
- [56] Gamboa O L *et al.* 2014 Working memory performance of early

ms patients correlates inversely with modularity increases in resting state functional connectivity networks *NeuroImage* **94** 385–395
<http://dx.doi.org/10.1016/j.neuroimage.2013.12.008>

